CORROSION & PREVENTION 2013

CONFERENCE & EXHIBITION

Where Theory Meets Practice

Brisbane Convention & Exhibition Centre

10–13 November 2013

www.acaconference.com.au

Major Sponsor:

ANTICORROSION TECHNOLOGY

Sustainable materials engineering and anti corrosion solutions

STOPAQ®

Self-healing corrosion prevention & sealant systems

A SEALFORLIFE COMPANY

Proudly Presented by:

Australasian Corrosion Association Inc.

Supporting Sponsors:

Dulux® Protective Coatings

International®

PPG Protective & Marine Coatings

RFS NDT

ABOUT THE PAPERS

Each manuscript published in these proceedings has been peer reviewed by industry experts selected from ACA's review panel. The ACA acknowledges the valuable contribution reviewers make to technical events such as these.

LIST OF PAPERS continued

THE AUSTRALASIAN CORROSION ASSOCIATION INC.

The Australasian Corrosion Association Inc. (ACA) was established in 1955 to service the needs of Australian and New Zealand companies, organisations and individuals involved in the fight against corrosion. It is dedicated to protecting the environment, ensuring public safety and reducing the economic impact of corrosion.

A membership based, not-for-profit, industry association, the ACA promotes the co-operation of academic, industrial, commercial and governmental organisations in relation to corrosion and its mitigation and for disseminating information upon all aspects of corrosion and its prevention by promoting lectures, symposia, publications and other activities.

The strength of the ACA lies in the great breadth of industry experience and academic training of its members; the common interest of which is the desire to increase effectiveness in controlling corrosion. Consequently, education and training, technical meetings and conferences and the distribution of the bi-monthly technical publication Corrosion & Materials are regular and necessary activities to disseminate information and technological advance. ACA encourages its members to become involved in other industry based organisations and utilises its membership base to achieve appropriate representation to bodies such as Australasian Standards organisations and State Electrolysis Committees. The ACA is a founding member of the World Corrosion Organisation and has been recently inducted into the European Federation of Corrosion.

The ACA holds an annual conference in November, providing a forum for industry professionals to present and discuss the latest in corrosion prevention methodology, products and cutting edge research. Approximately 100 peer reviewed papers are presented on a range of issues within technical streams such as infrastructure, concrete and concrete structures, coatings, cathodic protection, science and more.

On joining the ACA, members may select membership of up to five of ACA's eight Technical Groups. These Groups provide a structure for technical activities within a segment of industry or technical expertise, and were created from and formed for the benefit of members and Industry.

The seven Technical Groups are:

- Concrete Structures & Buildings
- Cathodic Protection
- Coatings
- Mining Industry
- Petroleum & Chemical Processing Industry
- Research
- Water and Water Treatment

Membership of the ACA is available to anyone with an interest in corrosion and its control. There are four categories of membership: Corporate, Individual, Student and Retired.

For further information on the ACA, please refer to www.corrosion.com.au or contact the ACA direct on +61 3 9890 4833 or aca@corrosion.com.au

BEHAVIOUR OF GRADE 310H STAINLESS STEEL EXPOSED TO HIGH TEMPERATURE HYDROCARBON PROCESSING GASES

I. Cismaru[1], A.J.McLeod[1], K. Duan[1], and R.E. Clegg[1,2]
[1] Central Queensland University, Gladstone, Australia [2] Bureau Veritas Asset Integrity and Reliability Services Pty Ltd, Brisbane Australia

SUMMARY: This paper presents the preliminary results from a study on the degradation behaviour of a bundle of heat exchangers tubes made from grade 310H stainless steel exposed to high temperature hydrocarbon processing gases. After fourteen months in service, the tubes were removed and examined to determine the degradation levels of the material. It was found that the long term exposure of the tubes to hydrocarbon gas with elevated temperatures up to 800°C had led to the precipitation of sigma phase and carbide. The environmental attack on the tube surfaces was also examined and the attack levels were mapped throughout the tube bundle. Furthermore these experimental results are discussed in terms of the degradation mechanisms and applications of metallic materials in this particular environment.

Keywords: Austenitic Stainless Steel, Sigma Phase, High Temperature Corrosion, Carburisation.

1. INTRODUCTION

High temperature corrosion is a matter of concern in high temperature gas processing. As well as damage caused by elevated temperatures, hydrocarbon gases can also lead to carburisation of the material and impurities in the gases such as sulphur can lead to other degradation mechanisms [1, 2]. High temperature oxidation is also a key degradation mechanism that can take place not only in the highly oxidizing atmosphere such as air or oxygen but also in environments containing sulphur dioxide and carbon dioxide with relatively low oxidation potentials. In general, many alloys are designed to combat a range of degradation mechanisms, most particularly, oxidation and carburisation.[3]

One of the most common mode of corrosion is a result of the attack of sulphur compounds, which, at high temperatures will react with the surface of the metal leading to metal sulphides, hydrogen sulphide and certain organic molecules [3]. It is well known that sulphur is a relatively strong corrodent and by comparison with the oxidation reaction, sulphur attack is a much more rapid corrosion process. This is due to factors such as higher diffusion rates in sulphides compared to those in oxides, tendency to form low melting point eutectics especially for nickel or nickel-based alloys, low solubility of sulphur, little difference in the free energy of metal sulphides formation and high dissociation pressure of sulphides.[3, 4]

Sulphidic corrosion can occur in reducing atmospheres due to the sulphur containing compounds being present in H_2 and/or hydrocarbon based atmospheres. In such atmospheres the organic sulphur compounds in feed stocks convert to H_2S and the corrosion becomes a function of H_2S concentration (or partial pressure).The combination of H_2S and H_2 in some processes can be particularly corrosive, and in this case, austenitic stainless steels are recommended for effective corrosion control. In general, nickel alloys are rapidly attacked by sulphur compounds at elevated temperatures, while chromium containing steels provide excellent corrosion resistance [3]. However, a practical alloy with superior sulfidation resistance has yet to be developed [4].

It is well known that in various series of stainless steels, the formation of undesirable secondary phases can occur after a long term exposure to temperatures between approximately 600 and 900° C [5, 6]. Among all the intermetallic phases that often precipitates in stainless steels, the process of σ-phase formation in austenitic stainless steels has formed the subject of a considerable number of research papers [7-17]. Austenitic stainless steels (class 300 e.g.: AISI grades 310, 316, 317) are susceptible to sigma(σ)-phase formation due to the molybdenum additions in AISI 316 and 317 and the high chromium content of AISI grade 310 (24-25%)[16]. From all the commercially produced Cr-Ni austenitic steels, 25Cr- 20Ni steels (e.g. grade 310) demonstrate the greatest susceptibility to σ-phase formation[9, 10]. Generally, the process of σ–phase formation is slow and is associated with the embrittlement of the steel at room temperature. Sigma- phase is known to have an important impact on mechanical and corrosion properties[5, 18] affecting the tensile and creep ductilities of the stainless steels[19]. Creep deformation under stress, accelerates σ–phase precipitation and extends its range to lower temperature[8]. Temperature is not the only parameter promoting the precipitation of σ–phase. Sigma formation kinetics are also affected by alloy chemistry, grain

size and the presence of secondary phases [10, 20]. In austenitic stainless steels, the tendency for σ–phase formation depends on the chemical composition of the residual austenite after precipitation of carbides and nitrides which always form first [10]. The σ-phase has a higher content of chromium and molybdenum than the austenite phase; therefore, the formation of σ-phase is always associated with a reduction of chromium and molybdenum in the nearby matrix. As this happens at the grain boundaries it provides an easy pathway for oxidation. The well demonstrated consequence of this is that, in addition to a decrease in ductility, there is a drastic worsening in corrosion resistance [6, 21].

This paper presents the preliminary results from a project aimed to investigate the performance of candidate materials for the furnace equipment exposed to high temperature hydrocarbon processing gases. The furnace used in the technological process consists of a number of tubes, piping and gas distributors, which the highly corrosive hot gas with a temperature in the range from 600 to 800 ºC will pass through and after that it is used as an energy source. Therefore, the tubes and fittings in these heat exchangers must be made of high temperature and corrosion resistant metals, to possess a good resistance to attack by both sulphur and carbon on their inner surface. They must also be resistant to creep deformation (under their own weight), sigma phase embrittlement and the oxidation of their external surface, which is exposed to a natural gas flame. This study is part of an experimental program that included both in-situ exposure and laboratory experiments and has been designed to help identifying and select the most cost-effective materials for use in hot reheat furnace tubes, to resist the combination of gaseous environment and temperature profile.

Previous studies had identified a range of candidate high-temperature corrosion resistant alloys for these components, which included stainless steels and nickel-base alloys. There are known variations in performance among the materials which were to be studied. The ultimate intention of this study is to understand the performance of the candidate materials in the furnace in order to choose the most cost effective material for the application. The previous studies identified that two main degradation mechanisms were expected. The first is the high temperature corrosion of the materials exposed to complex hydrocarbon-based gases. The second is the formation of deleterious phases (sigma, pi and laves) due to long term exposure to temperatures in the region of 800°C.

This paper reports on the results of examination of one of the candidate materials, grade 310H. The composition of the alloy is shown in Table1. A set of gas reheat furnace tube bundles were made from grade 310H stainless steel and were put into service in the demonstration plant. The plant operated for 14 months before the bundles were removed and at periodic intervals, the condition of the tubes was monitored using replicas. During the life of the tubes, the furnace temperatures were monitored and the gas compositions were periodically analysed. At the end of the service period, the tubes were removed for examination to determine the extent of degradation due to the two mechanisms: high temperature corrosion and intermetallic phase formation. This work enables an insight into the behaviour of grade 310H stainless steel to be obtained from in-service material under a relatively controlled set of conditions and will hopefully assist in the selection and design of better alloys for these applications. The approximate composition of the tube-side gas is as shown in Table 2.

Table1. Chemical Composition of the tested material

C	Mn	Si	S	P	Ni	Cr	Mo
0.05	1.55	0.56	0.0008	0.024	19.20	24.70	0.36

Table 2 Approximate composition of tube-side gas.

Component	H_2	CO	CO_2	N_2	H_2S	NH_3	H_2O	Misc Hydrocarbons
Mole %	20	11	15	1	2	<1	8	remainder

2. EXPERIMENTAL PROCEDURE

The tube bundles were examined visually for features relevant to manufacture, fabrication and surface attack. Representative locations were chosen for the following tests:

2.1 Metallographic Preparation and Examination

Transverse sections from the tube bundles were mounted in thermosetting phenolic resin and were prepared to a 1µm diamond finish in accordance with ASTM E3 [22]. The samples were examined in the unetched condition prior to etching with a variety of etchants. To reveal precipitates, the samples were etched by means of two different etchants: Vilella's Reagent and electrolytic 10% oxalic acid. Electrolytic etch was performed at 6V trying both etching techniques: swab and immersion. The majority of samples were treated with the immersion technique for 3 seconds [23]. The microstructure was examined by optical microscopy at magnifications up to 2000X.

2.2 Scanning Electron Microscopy (SEM) and Energy-Dispersive Spectroscopy (EDS)

The metallographic sections were examined using a JEOL JSM 6360 LA, scanning electron microscope. A JEOL Minicup Energy Dispersive Spectroscopy (EDS) detector was used to analyse the specimens and map the chemical composition across the samples.

2.3 Standard Test Method for Determining Volume Fraction by Systematic Manual Point Count

The volume fraction of identifiable phase (carbides, sigma etc) from sections through the microstructure was statistically estimated by the method of systematic manual point counting by means of a point grid. A 100 point square grid was superimposed over the micrograph and the number of test points falling within the phase or constituent of interest were counted and divided by the total number of grid points yielding a point fraction, expressed as a percentage, for that field. The average point fraction for n measured fields gives an estimate of the volume fraction of the constituent. The number of fields was chosen to reduce the 95% Confidence Interval (CI) below ± 1.5% (absolute)[24].

2.4 Flattening Test for Ductility

A flattening test was carried out to evaluate the ability of test pieces cut form tubes to undergo plastic deformation by flattening, to reveal the ductility of the tubes. The test was performed using the compression machine, under a load not exceeding 3 tonnes (30kN).

3. RESULTS AND OBSERVATIONS

3.1 Visual Examination and Details about Selection and Cutting of the Representative Locations on 310 H Tubes

The tube bundles varied somewhat in colour as the cooler tubes (9) containing the incoming gas were red and the hotter tubes were the blue-grey. The samples removed for destructive examination as shown in the Figure 1 are detailed below:
Four straight tubes numbered: 1, 3, 6, 9 and the elbow 3 corresponding to Tube 3 have been cut for metallurgical examination. According to the furnace temperatures data provided by the industry partner, the highest temperatures are reached on the Tube 1 and the second hottest is Tube 3. For this reason, more detailed examination has been undertaken on these two tubes i.e. the quarter points. The cooler tubes in the furnace, designated 6 and 9 were samples at mid length only as shown in the Figure 1.

At each location, two rings were cut. The first ring width was about 10 mm in the axial dimension and was used for

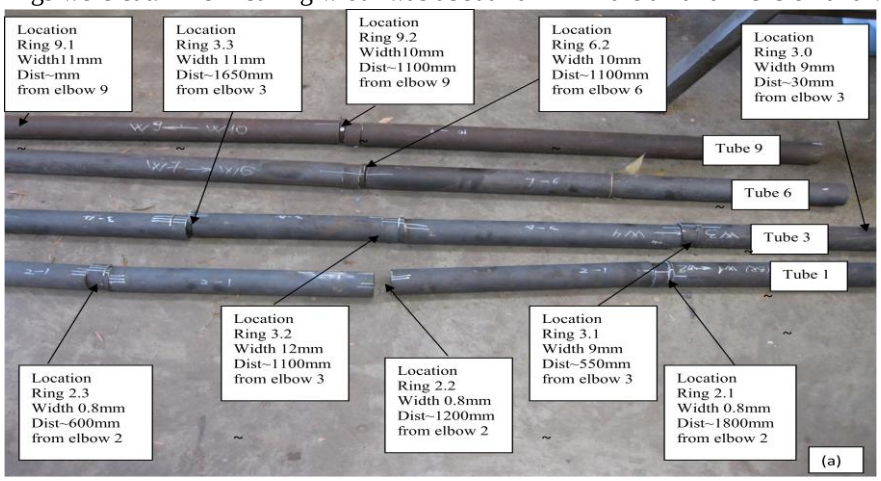

Figure 1 Position of samples from the tubes.

metallographic examination. The second ring had a width of 35 mm and was used for the flattening test. To identify variations (if any) around the circumference, particularly if the side facing the heat is hotter, four samples were cut from ring 2.2(mid length of Tube 1).

Some discoloration of the inside of the tube was found in some sections. Also, some of the tubes showed some evidence of blistering on the internal surface, as shown in Figure 2.

From the plant data, it was possible to determine the approximate temperature profiles of Tubes 1 and 9. An analysis of the data indicated that the tubes were exposed to variable temperature profiles, due to operation of the plant. The approximate figures for the time spent at each temperature are shown in

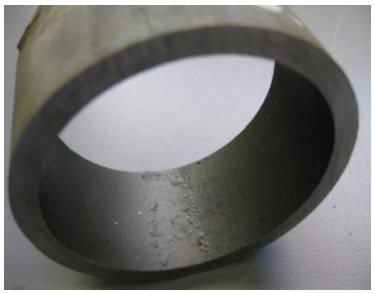

Figure 2 Some of the tubes showed evidence of blistering on the inside of the tube.

Table 3.

Table 3 Summary of the temperature profile experienced by the tubes over a 130 day period

Tube 1		Tube 9	
Temperature	Number of days	Temperature	Number of days
780-785	13	380-390	11
730-740	21	360-370	30
705-710	38.5	350-358	60
675-685	55.5	338-345	27
635	2		

3.2 Optical Metallography

As shown in Figures 3a to 3c, sigma phase particles were identified by their shape at locations from tubes 1, 3 and 6, along grain boundaries and at the triple points as indicated by the arrows. Widmanstatten precipitates occurred within grains. The intragrain Widmanstatten precipitates were deduced to be carbides. These were most prominent in Tube 1, which was exposed to the highest temperatures as listed in Table 3 . In Tube 6, the intragrain carbides had more or less disappeared, although sigma phase formation could be evidenced. In Tube 9, which was exposed to the lowest temperature among the tubes, the grain boundaries were highlighted in the microstructure, but no evidence of sigma phase formation could be seen (Fig 3d).

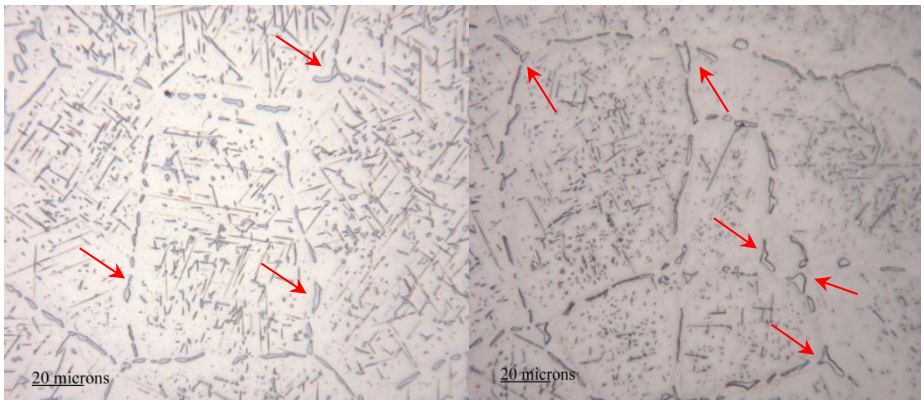

(a) (b)

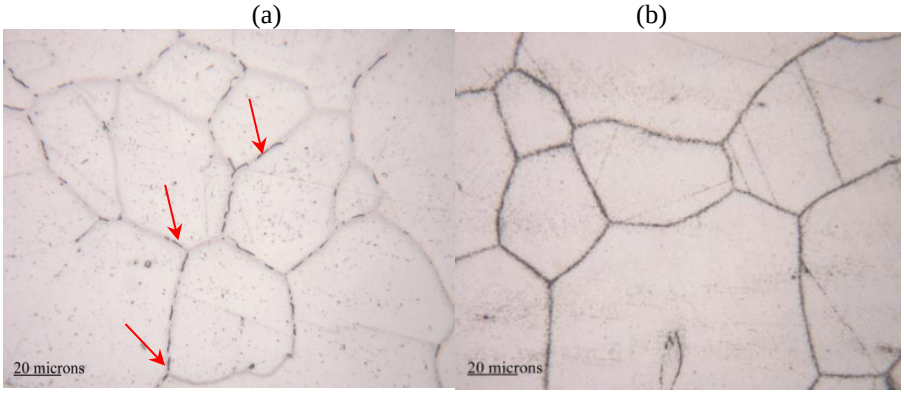

(c) (d)

Figure 3 a to d. Representative photomicrographs of locations from a. Tube 1, b. Tube 3, c. Tube 6 and d. Tube 9 (electrolytic etched 10% oxalic acid, 3 sec, 6V).

Sample 2.2 was cut from Tube 1 at the mid length and this was the hottest part of the tube bundle. Although direct measurements of the tube temperatures were not taken, the exit temperature of the furnace gas was measured and it was deduced that the operating metal temperature for Tube 1 was as shown in Table 3. Sections were taken from around the circumference of this tube and are shown in Figure 4 a to d. No noticeable variation in microstructure was identified around the circumference of ring 2.2, suggesting that the temperature profile about the ring was relatively uniform.

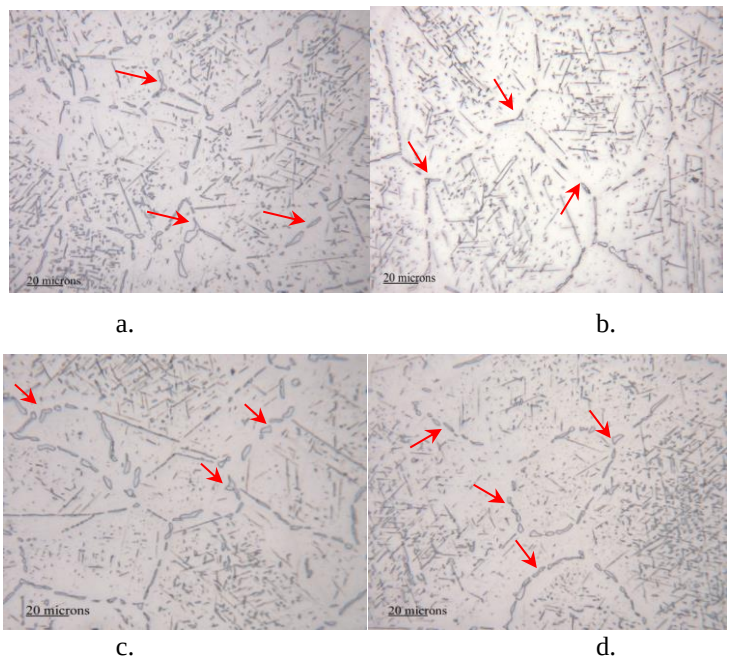

Figure 4 a to d. Micrographs taken about the circumference of the rings at the 0, 90, 180 and 270 degree positions about Tube 1 at position 2.2 (electrolytic etched 10% oxalic acid, 3 sec, 6V). Sigma phase areas are arrowed.

3.3 Standard Test Method for Determining Volume Fraction by Systematic Manual Point Count

The point counting was carried out to estimate the volume fraction of identifiable phase (carbides, sigma etc). The point counting only included the grain boundary phases and the Widmanstatten carbides were ignored at this stage. This was due to the difficulties in satisfactorily resolving the intragrain carbides. The results can be seen in Table 4. Each measurement was the result of 14 fields of reading for each specimen.

For the samples from the circumference of ring 2.2, the volume fraction values overlap and are within experimental uncertainty. The volume fractions were measured at four points about the circumference of the tube. These were labelled Upper (2.2 U), Lower (2.2 L) Inner (2.2 I) and Outer (2.2 O) and represent the quadrants about the circumference of the tube. Inner refer to the inside of the furnace and Outer refers to the side of the tube away from the inside of the furnace (away from the flame). As a result, it can be concluded that the damage to the tube was relatively uniform around the circumference of the tube. The values of the volume fractions determined a maximum of 6.0% identifiable phases in the hottest region of the tube bundles. The volume fraction decreases as the tubes become cooler. Although there were marginal differences in volume fraction, these were not considered to be statistically significant.

Table 4 Volume fraction determined by Systematic Manual Point Count

Sample number	Vol. Fraction (%)	95% CI	95% Interval	No of readings, n
2.1I	3.0	± 0.7	2.3-3.7	14
2.2U	4.9	± 1.0	3.9-5.9	14
2.2L	5.9	± 1.5	4.4-7.4	14
2.2O	5.0	± 1.5	3.5-6.5	14
2.2I	6.0	± 1.1	4.9-7.1	14
2.3I	5.9	± 1.0	4.9-6.9	14
3.0	3.8	± 0.9	2.9-4.7	14
Elbow 3	3.6	± 0.8	2.8-4.4	14
3.2I	4.1	± 1.6	2.5-5.7	14
6.2I	4.6	± 1.1	3.5-5.7	14
9.1I	3.3	± 1.0	2.3-4.3	14
9.2U	4.1	± 1.0	3.1-5.1	14

3.4 Scanning Electron Microscopy (SEM) and Energy-Dispersive Spectroscopy (EDS)

The particles identified as carbides and sigma phase in 3.2 were confirmed, through EDS analysis, as having high chromium content as expected in both these constituents. In addition, the EDS system was able to confirm the presence of carbon (coke) in the scale on the inside of the tubes, as well as sulphur. Figure 5 shows the maps of chemical composition for a region near the inner surface in the samples from Tube 1. As can be seen from the EDS mapping in Figure 5, the grain boundaries are deficient in Cr whereas more Ni and Fe were found. This was balanced by more Cr in the scale, due to its higher affinity with oxygen and in particles, due to its nature to form carbides. There was some evidence of Cr depletion towards the inner surface of the tube, with Cr accumulating in the scale. No evidence of sigma phase was found in the Cr-depleted surface layers such as in Fig 4. Sulphur was also detected in some particles in this surface layer and some evidence of sulphidation attack to a depth of approximately 30 µm was seen. However, this appeared to be the limit of sulphidation attack in this component.

Sample 6.2 I from Tube 6 was also studied and some evidence of grain boundary penetration was seen. This was generally less than 20 µm deep, however. Again, Cr tended to deplete near the surface of the tube, but Cr partitioning was less than that observed on Tube 1. EDS elemental mapping was also done on sample from Tube 9 however the results did not indicate that significant partitioning of elements was occurring on this sample.

Elemental analysis by EDS on elbow 3 as shown in Table 5, revealed high sulphur content on the scale at the inner surface as shown in Figure 6. For the sample 6.2 I cut from the middle of Tube 6, as shown in the Figure 7 the chemical analysis by EDS revealed the presence of sulphur in the scale. In addition, carbon (coke) was detected in the scale, possible the presence of particles of contamination (grinding swarf) as shown in Table 6.

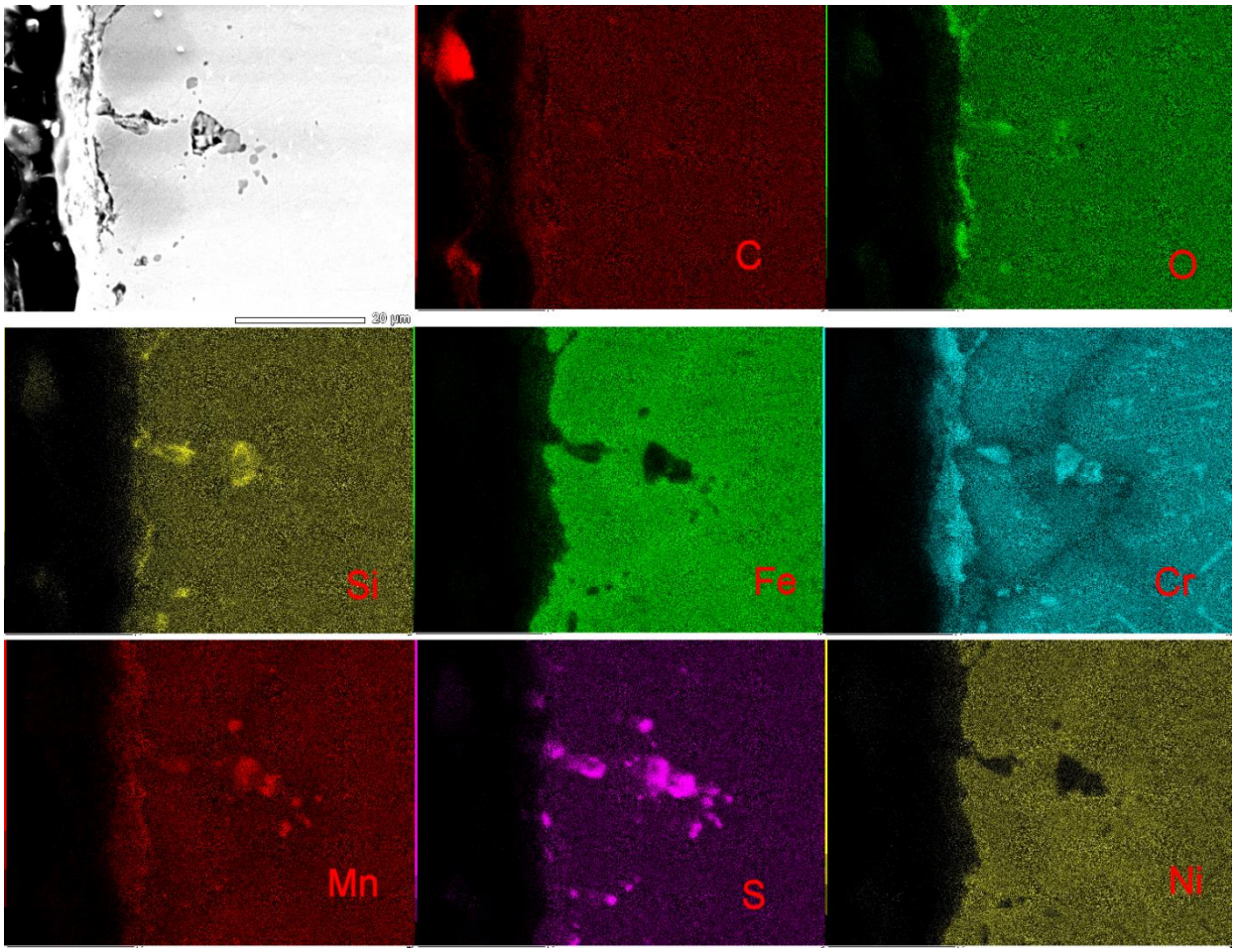

Figure 5 EDS elemental maps of the tube-side surface of tube 1 (position 2-2).

The results given in Table 5 are interpreted as follows. The metal near the surface (009, 011 to 014) has been depleted in Cr, but the precipitate particle (010), carbide or sigma phase, is still high in Cr. The light scale in contact with the metal (001-008) is Fe-Cr oxide. The darker, more remote scale is mainly carbon (coke) with Fe, Ni, Cr sulphide. Perhaps some free sulphur. The intermediate scale is carbon (coke) with Ni, perhaps in the form of sulphide. (Ni does not form carbide.)The elements in the cavity suggest metallic carbide and sulphide. This was not studied further.

The analysis results as shown in Table 6 are interpreted as follows. The carbon (coke) contains elemental carbon and metallic sulphides. The grain boundary attack has oxide also. The source of Na and Al is not known. In the gap are tramp particles and elements which were not studied further.

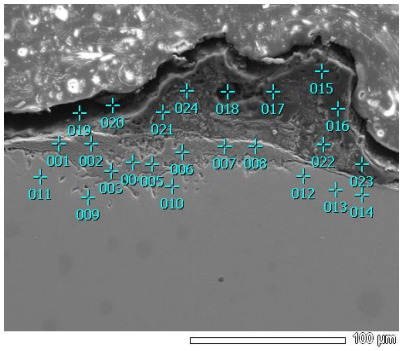

Figure 6- SEM view of sulphur attack at the inner surface cross –section of elbow 3 showing results of chemical analysis by EDS

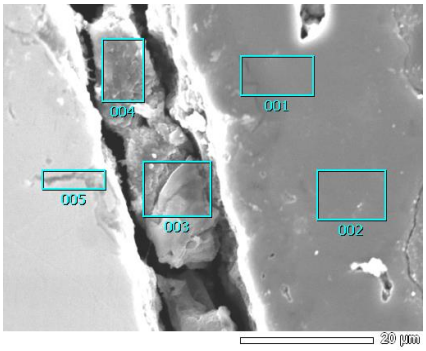

Figure 7 - SEM view at the inner surface on sample 6.2 I showing results of chemical analysis by EDS

Table 5-Chemical analysis by EDS on sample from Elbow 3(From Figure 6) (in wt%)

Element	Metal near surface	Metal near surface-precipitate particle	Light scale in contact with metal	Light scale in contact with metal	Intermediate scale	Dark scale more remote	Cavity
Analysis No.	009, 011-014, 024	010	001, 004-008	002-003	021-023	015-017	018-020
C	-	1.2	1-9	1-3	53-86	85-90	12-23
O	-	-	7-11	11.5-12	1-3	2-6	<2
Al	-	-	-	-	-	-	0.4-0.6
Si	0.1-0.9	0.9	≤1.3	0-0.8	<0.5	≤0.6	3-13
S	-	-	2-10	≤0.9	5-13	4.5-5.4	11-16
Cr	11-27	35	40-62	56-64	0.8-1.5	0.3-1.1	11-15
Ni	17-23	9	<1	<1	0-19	0.6-0.8	10-14
Fe	Rem.	Rem.	15-37	17-26	3-25	1.5-2.1	26-40

Table 6 -Chemical analysis by EDS on sample 6.2I from the mid length of Tube 6 (From Figure 7)

Element	Carbon (coke)	Attack on grain boundary	Swarf trapped in gap
Analysis No	001-002	005	003-004
C	92-93	2	5-54
O	-	3	3-15
Si	-	1.5	0.5-2.7
S	2.0-2.8	0.4	3-6
Cr	0.4-0.6	21	7-16
Ni	0.4-0.6	19	3-13
Fe	3.0-3.5	50	14-48
Other		0.3 Na, 0.2 Al	0.9-1.8 Na, ≤0.4 Al 1-1.5 Ti ≤0.5 Cu

3.5 Ring Flattening Test

In order to evaluate the ductility of the grade 310 H stainless steel metallic tubes after 14 months' service, a flattening test was performed, followed by a visual inspection in order to observe the damage (if any) evident in the surface of the tubes. Ring samples of 30 mm in length were flattened between parallel plates. If no fracture was observed, mandrels were inserted to increase the bending deformation in the tube wall until opposite walls of the rings met.

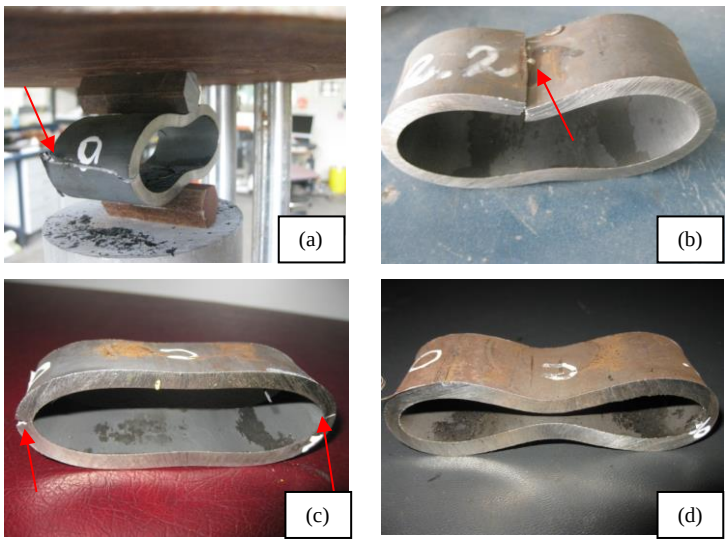

Figure 8. Flattening test on ring: (a)- 2.1, (b)-2.2,(c)-2.3,(d)-9

Table 7 – Flattening test results and observations

Sample number	Flattening Test Observations
2.1	Cracked on one side
2.2	Cracked from the inside(the worst crack)
2.3	Cracked on both sides
3.1	Fissure on the tension surface , didn't extend to the edges, not visible in the Fig.
3.2	Fissure on the tension surface , didn't extend to the edges, not visible in the Fig.
3.3	No crack
6.2	No crack
9.2	No crack

Figure 8 and Table 7 show the failure modes and critical loads of ring specimens from different locations. The flattening test results showed that corresponding to a temperature difference of about 300 to 400 °C, the maximum temperatures of 640 to 790 °C at Tube 1 and the low end of 340 to 390 °C at Tube 9, the tube failure modes have changed from brittle fracture to complete ductile failure. This can be seen in Figure 8 and Table 7, where obvious crack developments can be seen in specimens 2.1 to 2.3, which were exposed to higher temperatures (those samples failed the flattening test), and the specimens 3.3, 6.2 and 9.2 exposed to lower temperatures had no crack initiation and growth until the entire ring specimens were completely flattened.

An SEM fractographic examination has been performed on ring 2.2 (from Tube 1), in which fracture occurred after significant deformation in the flattening test as shown in Figure 9 (a)-(d). Whilst the fractures were predominantly by a ductile overload microvoid coalescence mechanism, some intergranular fissures were seen, as indicated by arrows. In Figure 9(b), it is apparent that there were a number of hard particles on the fracture surfaces. These were probably carbide particles. The fracture surfaces indicated that at the higher exposure temperatures, fracture was predominantly intergranular and crack paths were driven largely by the carbides and other intermetallic compounds on the grain boundaries.

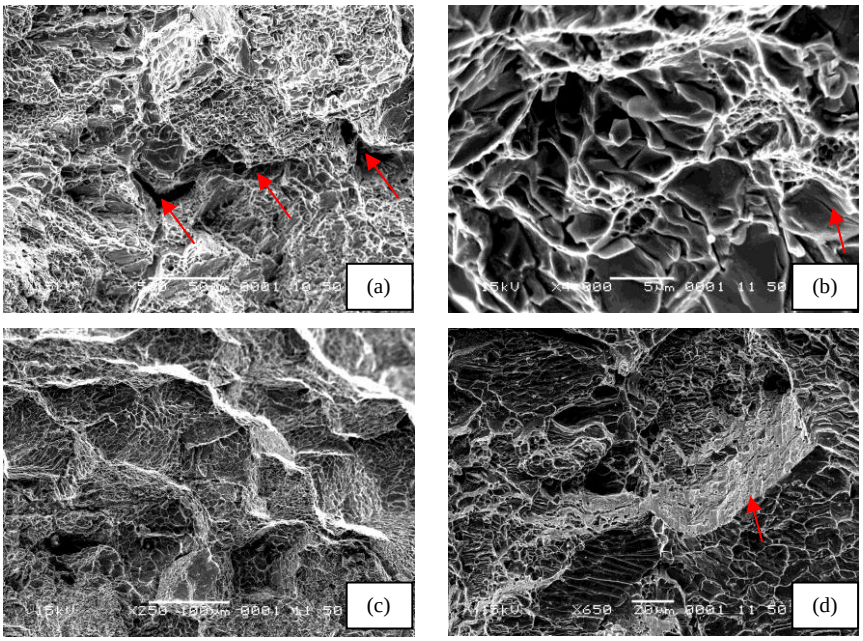

Figure 9 SEM views- Fractographic examination on ring 2.2 after failed the flattening test:(a)-Intergranular fissures, non-random ductile fracture involving coalescence of voids (b)- hard particles, brittle fracture, typical crack (river mark) on hard particles as indicated by the arrow, (c)-intergranular cracking(d)- grain boundary facet

4. CONCLUSIONS

SEM-EDS indicated that the tube bundles were made from a material consistent with AISI 310 H stainless steel. The microstructure of 310 H stainless steel had become degraded by the operation at high temperatures for a period of time of 14 month, especially in the hottest part of the tubes.

The tube bundles had become carburised and this resulted from the bundles operating in a reducing atmosphere. The change in volume fraction of the carbides at higher temperatures was probably the result of increased carburisation at the elevated temperatures. Carburisation had made the tubes brittle and cause fracture along intergranular planes. At this stage, only flattening tests have been carried out, however, it is expected that a similar trend with higher exposure temperatures would be seen using Charpy impact tests.

On the hottest portion of the tubes (Tube 1), the evidence of sulphidation attack was found, with some sulphidation penetrating up to 30 µm. However, this level of sulphidation was less than that was originally expected, possibly indicating that the H_2S content of the gas stream was less than expected. Noticeable sulphur attack was also found in mapping for Tube 6 but not as significant as the one from Tube 1. In addition, coke (carbon) was detected in the scale, possible the presence of particles of contamination (grinding swarf). The tubes had also oxidised on the surface.

There was evidence of sigma phase formation observed in the micrographs taken from Tubes 1, 3 and 6. This represents the higher temperature portion of the 310 H stainless steel tube and associate pipework. According to the same micrographs the microstructure was as expected and consisted of austenite with minimal retained ferrite and carbide precipitates.

The absence of massive grain boundary sigma phase or Widmanstatten carbide in sample 9.2 is consistent with the lower operating temperature. The pass [i.e. not fail] in the Tube flattening bend test indicates that the grain boundary changes have not affected ductility.

5. ACKNOWLEDGMENTS

The authors would like to thank the industry partner for the financial support of this project. Without their help, this research work would not have been possible. They are also obligated to thank Professor David Young from the University of New South Wales for useful and interesting discussions and for his scientific guidance about this research project.

6. REFERENCES

1. Lai, G.Y., *High Temperature Corrosion of Engineering Alloys*. 1990: ASM International. 231.
2. Lai, G.Y., *High Temperature Corrosion and Materials Applications*. 2007: ASM International. 477.

3. Khanna, A.S., *High Temperature Oxidation and Corrosion*. 2002: ASM International. 324.
4. Young, D., *High Temperature Oxidation and Corrosion of Metals*. Vol. 1. 2008: Elsevier. 574.
5. Babakr, A., et al., *Failure Investigation of a Furnace Tube Support.* Journal of Failure Analysis and Prevention, 2009. **9**(1): p. 16-22.
6. Kington, A.V. and F.W. Noble, *σ phase embrittlement of a type 310 stainless steel.* Materials Science and Engineering: A, 1991. **138**(2): p. 259-266.
7. Cieslak, J., Reissner, M.,Steiner, W.,Dubiel, S.M., *On the Magnetism of the Sigma Phase Fe-Cr Alloys.* Physica Status Solidi 2008. **(a)205**(8).
8. Barcik, J., *The kinetics of σ-phase precipitation in AISI310 and AISI316 steels.* Metallurgical and Materials Transactions A, 1983. **14**(3): p. 635-641.
9. Barcik, J., *The Process of σ-Phase Solution in 25Cr-20Ni Austenitic Steels.* Metallurgical Transactions 1987. **18A**: p. 1171-1177.
10. Barcik, J., *Mechanism of σ–phase precipitation in Cr-Ni austenitic steels.* Material Science and Technology, 1988. **4**: p. 5-15.
11. Barcik, J., Journal Applied Crystallography, 1983. **16**.
12. Blenkinsop, P.A., Nutting,J., Journal Iron Steel Inst., 1967. **205**.
13. Singhal, L., K. and Martin,J.,W., *The formation of ferrite and sigma-phase in some austenitic stainless steels.* Acta Metallurgica 1968. **16**(12).
14. White, W.E. and I. Le May, *Metallographic observations on the formation and occurrence of ferrite, sigma phase and carbides in austenitic stainless steels. Part III. Electron microscopy studies.* Metallography, 1972. **5**(4): p. 333-345.
15. Goldschmidt, H.J., *Interstitial Alloys*. 1967, New York: Plenum Press 158-167.
16. Tavares, S.S.M., et al., *Microstructural changes and corrosion resistance of AISI 310S steel exposed to 600–800 °C.* Materials Characterization, 2009. **60**(6): p. 573-578.
17. Hull, F.C., *Effects of Composition on Embrittlement of Austenitic Stainless Steel.* Welding Journal, 1973. **52**(3): p. 104s-113s.
18. Khatak, H.S. and B. Raj, *Corrosion of Austenitic Stainless Steels- Mechanisms, Mitigation and Monitoring*. 2002, India: Narosa Publishing House. 385.
19. Shaikh, H., Pujar,M.G.,Sivaibharasi,N.,Sivaprasad,P.V.,Khatak,H.S.,Materials Science and Technology, Materials Science and Technology, 1994. **10**.
20. Young, D., *Sigma Phase Embrittlement of 310 H Stainless Steel for QER Ltd*, 2010.
21. Terada, M., et al., *Investigation on the intergranular corrosion resistance of the AISI 316L(N) stainless steel after long time creep testing at 600 °C.* Materials Characterization, 2008. **59**(6): p. 663-668.
22. *Annual Book of ASTM STANDARDS E3-95* 1997.
23. *Annual Book of ASTM STANDARDS E407.* 1997.
24. *Annual Book of ASTM STANDARDS E562-95.* 1997.

Iuliana Cismaru is a qualified chemical engineer with more than 10 years experience in managing, design and installation of natural gas pipelines and networks. Currently she is a Masters Student at the Central Queensland University. She assisted the consulting effort of the PELM Centre at CQ University - Gladstone in metallurgical failure analyses of industrial components i.e. cracking, fracture, wear, corrosion, etc.